ADVANCED MATERIALS INTERFACES
www.advmatinterfaces.de

Polymer Brush Gradients by Adjusting the Functional Density Through Temperature Gradient

Bat-El Pinchasik, Klaus Tauer, Helmuth Möhwald, and Andre G. Skirtach*

The group of silanes is one of the most abundant classes of molecules used for surface modification. In most studies, silanization is made from the vapor phase or solution. Here, an easy, robust, and fast way not only to modify, but also to map, control, and predict the wetting profiles on silicon surfaces after silanization and the final characteristics of a brush layer polymerized from this silane template profile are presented. The initiator molecule, 2-bromo-2-methyl-N-3-(triethoxysilyl) propyl propanamide (BTPAm), is spin-casted on a silicon substrate and a thermal gradient is applied using a combinatorial approach for studying the influence of temperature on the spin-casted silanes. Subsequently, polyacrylamide (PAAm) brushes are grown from the initiating end group of the BTPAm molecules through atom transfer radical polymerization (ATRP). Simulations of the heat distribution inside the silicon wafer allow both confirming the mapping of surface properties and designing desired profiles by predicting thermal distributions. An analytical expression for quantification is also provided. Thus, the wetting properties, surface roughness, and morphology of the brush layer after polymerization are mapped and correlated with the initial BTPAm gradient profile. The studies presented are envisioned to be of interest for designing surface profiles with different wetting properties, facilitating polymer brush growth, and to be used as predictive tools.

1. Introduction

Gradient coatings offer two attractive functions: a) active coatings or functional substrates[1] and b) combinatorial studies. They can make a droplet run uphill[2] and cause cell migration.[3] They can also be used for combinatorial studies in systems with multiple variables to reduce numerous samples with varying characteristics to one sample with many possible combinations. Examples of gradient coatings for the combinatorial approach include cell adhesion and proliferation studies,[4,5] colorimetric applications,[6] fundamental studies of polymers[7] and interfacial phenomena.[8] In many studies on gradient coatings silanes are being used to modify the surface properties. Various examples can be found in the fields of organic and inorganic electronics,[9,10] optics and sensing,[11] active coatings,[12,13] catalysis[14–16] and biology.[17] In addition, silanes are commonly used as templates initiating growth of polymer brushes. These further expand the possible modifications of surfaces by introducing pH responsive coatings,[18] solvent or temperature responsive materials and templates for the fabrication of micro- and nano- structures.[19,20] For the deposition of silanes two main methods are mostly used. A very common one is deposition from solution.[21,22] This method requires anhydrous solvents and strict conditions with regards to humidity, temperature and purity.[23–26] Additionally, silane molecules are capable of polymerization in the bulk solution prior to deposition, forming oligomeric and polymeric chains. These bulky chains hinder the formation of reproducible smooth layers. Nevertheless, by tuning the silanization conditions, dense and smooth monolayers can be achieved.[22] To avoid these implications vapor deposition is used. However, in this method the obtained layer is greatly influenced by the vapor pressure of the molecules. Lower concentration of the silane molecules in the vapor phase in comparison to solution is believed to be the reason for the formation of weaker bonds between silanes and the substrate, resulting in poor film stability.[23] Both in deposition from solution and vapor repeatedly reported durations of the silanization last up to 48 h.[27,28] Spaying silanes in a custom made chamber was a suggested intermediate method[29] however, this method is less common, possibly because of technical aspects of constructing a special setup. In addition, some studies showed the fabrication of gradients and other patterned surfaces by selective chemical lithography.[30–32] There are significantly fewer examples of spin-casted silanes in comparison to silanization from solution or vapor. Some examples for this method were demonstrated in immobilization of DNA on glass[33] and construction of metal coatings.[34] Nevertheless, in

B.-E. Pinchasik, Prof. H. Möhwald
Max Planck Institute for Colloids and Interfaces
Department of Interfaces
D14476, Germany
E-mail: batel.pinchasik@mpikg.mpg.de
Dr. K. Tauer
Max Planck Institute for Colloids and Interfaces
Department of Colloid Chemistry
D14476, Germany
Prof. A. G. Skirtach
Ghent University
Department of Molecular Biotechnology & NB-Photonics
9000, Ghent, Belgium

DOI: 10.1002/admi.201300056

these studies the contribution of physisorbed or weakly bound silane molecules is unclear due to lack of thorough rinsing after spin-casting. In the field of organic electronics, octadecyltrimethoxysilane (OTS) was spin-casted on oxidized silicon substrate to form densely packed self-assembled monolayers.[35] In other studies the silicon substrate was immersed into silane solutions, thoroughly washed and thermally cured.[36] Overall, the influence of temperature on silane spin-coated substrates was not thoroughly investigated.

In this paper, we systematically study the silanization of spin-casted BTPAm via a combinatorial approach. We applied a temperature gradient to a spin-coated substrate for short time intervals, resulting in a linear relation between temperature and degree of silanization. In addition, polyacrylamide brushes were grown from the initiating end groups of the BTPAm. This enabled an estimation of the resulting polymeric layer thickness as a function of the initial silanization temperature. With this study we offer a fast, easy and reproducible method for mapping the degree of silanization and predicting wetting properties of spin-casted BTPAm. Our method can be applied both for tuning wetting properties and mapping the silanization dependence on temperature for spin-coated substrates. Furthermore, this technique can be potentially used for templating polyelectrolyte multilayers based on electrostatic interactions in case the silane molecules have charged end or side groups. Templating gradients of polyelectrolytes can be exploited for tuning the wetting properties,[37] surface charge[38] and be applied for manipulating the biocompatibility of surfaces.[39]

2. BTPAm Gradient Formation on Silica

In this study, 1 mM BTPAm in toluene is first spin-casted onto a silicon wafer, followed by applying a temperature gradient to the substrate (**Scheme 1**). The substrate surface area and spin-coating conditions were kept constant for all samples; hence we assume a fixed number of silane molecules on each substrate. While toluene evaporates, the BTPAm molecules remain on the substrate and are free to diffuse laterally. However, they are less mobile in comparison to silane molecules in solution, and polymerization prior to interaction with the surface might hinder their motion. Heating the substrate after spin-casting the BTPAm promotes silanization. It is important to stress that the samples after silanization are rinsed and sonicated for 5 min with toluene and therefore, all physisorbed molecules are no longer on the substrate and the remaining layer of BTPAm molecules is attached to the surface through a chemical bond. Higher temperature results in higher degree of

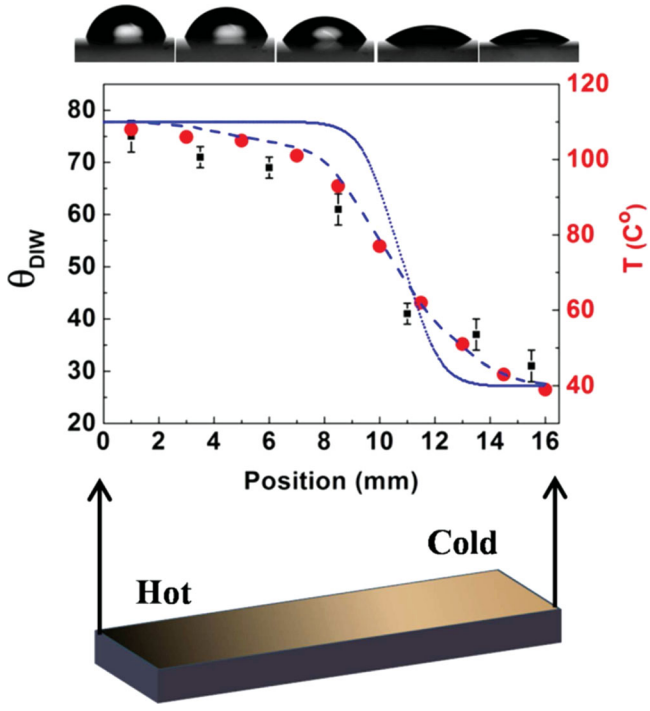

Figure 1. Top: optical images of water droplets along a silicon wafer (16 mm in length) taken at 2 mm, 5 mm, 8 mm, 11 mm and 14 mm from the hot side (quantitative data of contact angles are given in the graph below). Middle: graphs representing the measured water contact angle along the BTPAm density gradient (black squares), measured local temperature applied to the surface (red circles), simulated temperature profile inside the wafer (blue continuous line) in an ideal case and simulated temperature profile adjusted to the experimental conditions (blue dashed line). Bottom: schematics indicating the hot and cold sides of the silicon wafer.

BTPAm coverage, as deduced from contact angle measurements (**Figure 1**). The contact angle (black squares) varies by $\Delta\theta_{DIW} \approx 40°$ along the substrate. By measuring the local temperature (red circles) it was possible to correlate temperature and extent of silanization by BTPAm. This correlation was found to be linear. The blue dotted line (ideal case) is a simulated temperature profile for boundary conditions of 110 °C as the highest and 40 °C as the lowest temperature. The actual thermal profile (the blue dashed line in Figure 1) was obtained by fitting the experimental data (the red solid circles in Figure 1), which was made by splitting the heating stage into sub-stages (Experimental Section). It can be noted that heat losses along

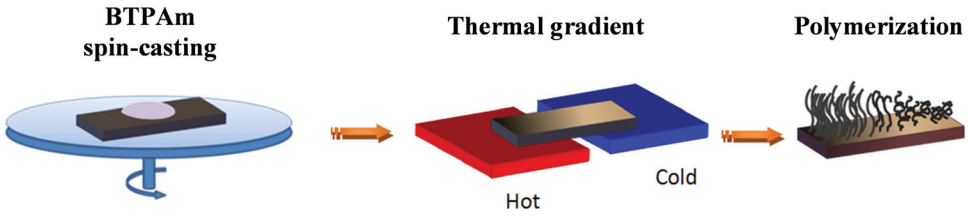

Scheme 1. Polymer gradient synthesis scheme: spin-casting of BTPAm (left), applying temperature gradient (middle), and polymerization of PAAm brushes (right).

the heating stage could account for such a situation. The simulation provides a reasonable depiction of the experimental data.

Uniform heating of BTPAm coated substrates resulted in $\Delta\theta_{DIW} = 32 \pm 2°$ for 115 °C and $\Delta\theta_{DIW} = 75 \pm 2°$ for 40 °C (see Silanization Mechanism Section in Supporting Information). This implies that no significant lateral diffusion is taking place on the macro-scale, as it was initially assumed, and heating only promotes micro-scale local silanization. Since the samples are thoroughly rinsed and sonicated with toluene after applying the thermal gradient, the remaining BTPAm molecules are covalently attached to the silicon dioxide rather than physisorbed or bound by hydrogen interactions. A study using a BTPAm monolayer as an initiating template for poly(ionic liquid) brushes yielded a contact angle of $\Delta\theta_{DIW} = 75°$ after immersing a silicon substrate in 10 mM BTPAm in anhydrous toluene for 4 h at 55 °C and then keeping it overnight at RT.[40] Another study dealing with functionalization of silicon nanowires reported a contact angle of $\Delta\theta_{DIW} = 85°$ after 12 h at 80 °C under inert atmosphere.[41] In addition, studies using BTPAm as an initiating template for growing polymer brushes repeatedly exposed the silicon surface to the silane solution for extended time intervals of up to 48 h, often at elevated temperature.[42–44] The similarity between contact angles of substrates prepared with prolonged dipping in silane solutions and spin-coated silicon substrate heated for 20 min at 120 °C implies that both methods result in the same surface coverage. No reported contact angle value for BTPAm coated silicon substrate exceeds the value of 85°, meaning there is an upper threshold for surface coverage and maximal packing of molecules for monolayers and submonolayers. We suggest that this coverage can be achieved already after 20 min at 120 °C for spin-coated substrate, instead of prolonged exposure to solution or vapors.

AFM images show different degree of coverage and aggregation between the two edges of the substrate (**Figure 2**). In each AFM image three topographical profiles (appear as white lines on the images with red, green and blue markers) are examined. The thickness along these profiles is presented below each image. Initiator was deposited with the temperature difference 120–30 °C for 20 min. While on the cold side, the distance between aggregated centers of BTPAm is in the order of hundreds of nanometers, the BTPAm layer on the hot side is more populated with initiator molecules, creating spaces of few dozens of nanometers and less between the aggregated centers. On both edges, the height of the aggregated islands is in the range of 1.2–1.5 nm, implying that the BTPAm molecules do not form multilayer stacks but a monolayer or a sub-monolayer. Considering an area averaged thickness of approximately 1.3–1.4 nm (see Thickness Measurement of Spin-Casted BTPAm Section in Supporting Information), it can be deduced that roughly 85% and more of the area on the hot side is covered with BTPAm. Although the reproducibitly and structural arrangement of silane monolayers for long time is an ongoing debate, nowadays it is commonly accepted that the model of heterogeneous "islands" surrounded by an unordered silane molecules "sea" describes silane layers (such as *n*-octadecyltrichlorosilane) in the case of deposition from solution.[45,46] This structure is evident from the hot side (120 °C) as seen in **Figure 3** (left). The ambient humidity was controlled and all experiments were performed at humidity values ranging between 36–38%. Humidity has the potential to change the morphology of the silane layer, however, since the silanization in this study is made over a broad range of temperatures, a different humidity will not necessarily diminish the aggregation completely. It is difficult to predict the final morphology of the silanization layer while the temperature changes by 90 °C over 16 mm. Previous studies show that partially hydrated substrate reduces aggregation of OTS molecules at 25 °C however, promotes aggregation at 9 °C.[24] It is important to stress that, although inhomogeneity exists on the micro scale, the macroscopic properties of the coated substrate were highly reproducible.

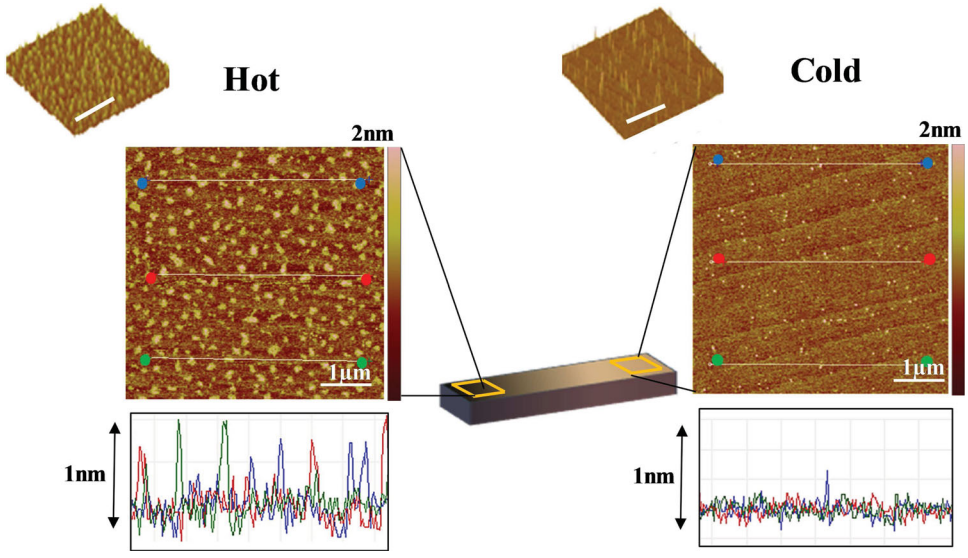

Figure 2. AFM images (with corresponding 3D images at the top left corners) and three representative height profiles (below) taken from different areas of the BTPAm layer after heating the silane coated Si substrate (120–30 °C, 20 min). Left: images and profiles taken from the hot side of the silicon wafer. Right: images and profile taken from the cold side.

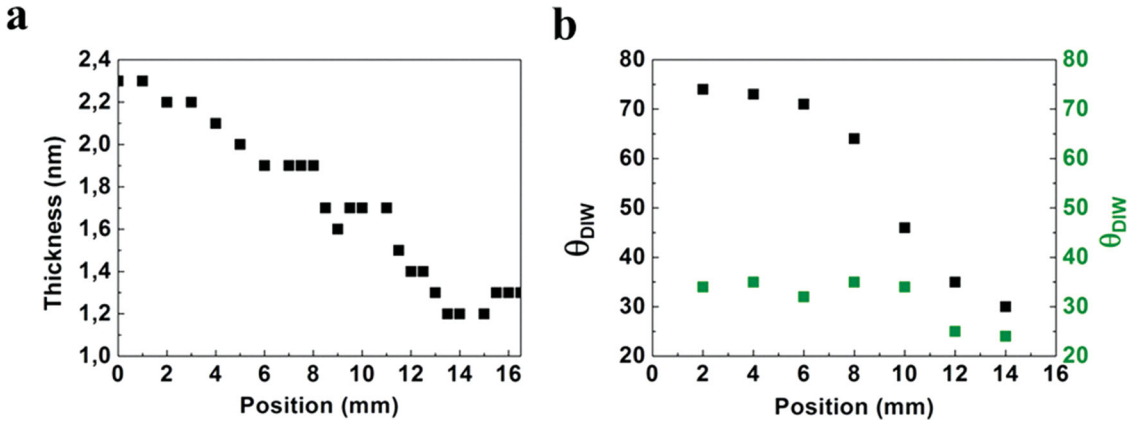

Figure 3. a) Thickness of PAAm brush layer (black squares), initiated from the BTPAm template. b) Contact angle of the BTPAm layer prior to polymerization (black squares), and water contact angle after polymerization of PAAm brushes (green squares).

3. Synthesis of Polymer Brushes

Initiator coated substrates were then polymerized via ATRP. Since the PAAm brushes are grafted from the initiator (BTPAm) gradient made in the second step in Scheme 1, their grafting density is changing according to the initiator template. It is assumed that the polymerized brushes do not vary in molecular weight. This is a realistic assumption, since no polymerization did take place, and it is in accordance with previous studies on density gradient polymer brushes.[47] Polymer brush coatings exhibit two main regimes: "brush" and "mushroom" regimes, depending on the grafting point density.[48] Ellipsometry measurements along the substrate heated with a 120–30 °C profile for 20 min (Figure 3a) revealed a linear decrease in layer thickness in the brush regime (0–13 mm) and the "brush-to-mushroom" transition (position of 13 mm). Previous studies conducted by Wu et al.[47] and Genzer et al.[49] showed that the thickness and wetting properties are independent of the grafting density in the mushroom regime. In the brush regime however, the polymer brush layer thickness varies depending on the grafting density, and therefore it is possible to distinguish between these two regimes. The results reported here agree with the previous studies in regard to wetting properties and thickness of the polymerized brush layer, and therefore it is possible to distinguish between the "brush" and "mushroom" regimes. In the same study, they reported calculated brush grafting density of 0.15 nm^{-2} in the dense part and 0.01–0.005 nm^{-2} in the sparse areas. It appears that the brush regime, where the brush layer is dense, corresponds to contact angles larger than 40° prior to polymerization. This contact angle is obtained for temperatures larger than 60 °C initially applied to the silane coated substrate. The brush-to-mushroom transition takes place where the contact angle before polymerization is approximately 40° ± 2°. Variation of the thickness in the "mushroom regime" can originate from variations in the initiator aggregates.

The drop in the contact angle values after polymerization (indicating the PAAm brush layer) in comparison to the initial contact angle values (indicating BTPAm layer) confirms the surface modification (Figure 3b). The contact angle in the brush regime has a maximal drop of 40°, indicating the formation of a dense PAAm layer on the hot side of the substrate. This stands in accordance with a former study reporting contact angles of 37 ± 2° for a homogeneous PAAm brush layer.[48] On the cold edge the contact angle changed from approximately 30 ± 2° before polymerization to 24 ± 2° afterwards since the water droplets can penetrate more easily in between the brushes, sensing the original substrate. The contact angles of the initiator template prior to polymerization are 75 ± 2° in average on the dense part and 37 ± 2° on the sparse part. We conclude that the water droplet used for the contact angle measurement does not penetrate the initiator layer on the dense side however does penetrate in between the initiator molecule islands or randomly distributed molecules on the sparse side. After polymerization the contact angle on the dense part drops to 35 ± 2° in average, approximately the contact angle of a smooth dense PAAm brush layer. Therefore, it is still assumed that the droplet does not penetrate in between the brushes. However, on the sparse side where the droplet is able to sense the silicon substrate, now there is an additional contribution of the PAAm brushes where initiator hydrophilic molecules used to be prior to polymerization. Hence, there is a further drop in contact angle from 30 ± 2° to 24 ± 2°. We assume that no degradation or hydrolysis of the silane layer occur during the polymerization since the stability of silane layers is enhanced when heated.[27] The wettability gradient loses its steepness after polymerization however, wettability reflects short range interactions while properties influenced by long range interactions such as friction may still vary significantly along the brush layer gradient. Also properties related to the film thickness like incorporation of dyes or reactants are expected to vary along the gradient. Previous studies showed the influence of grafting density on adhesive forces and intermolecular interactions[50] and the capture and immobilization of antibodies onto polymer brushes.[51,52] Studies along this line are promising but beyond the scope of this work. It is also possible to change the polymerization method from "grafting from" to "grafting to" as was demonstrated in previous studies.[53] This can further expand the resulting polymeric brush layer with respect to precisely predetermined molecular weights.[54] However, "grafting

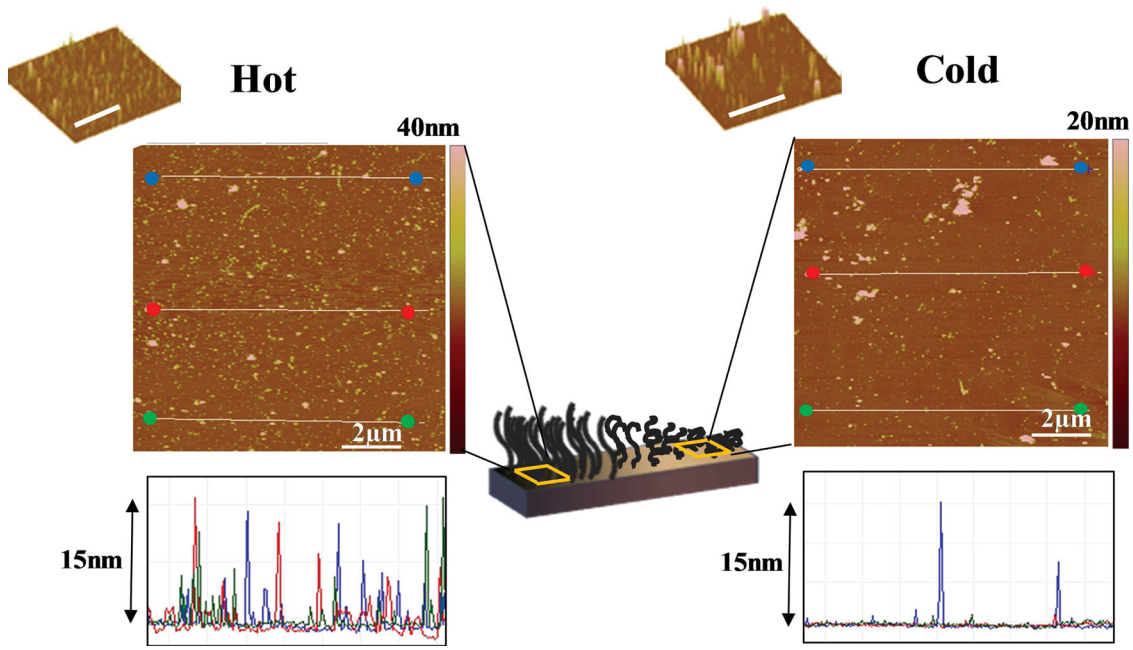

Figure 4. AFM images (with corresponding 3D images at the top left corners) and three representative height profiles taken from different areas of the PAAm brush layer (below). Left: images and profiles taken from the hot side of the silicon wafer. Right: images and profile taken from the cold side.

from" has the advantage of reduced steric hindrance during polymerization.

A roughness parameter is frequently used in studies of protein adsorption to substrates.[55,56] PAAm brush coatings are especially interesting since they can function as a biocompatible material be used for cell culturing and migration studies.[57–59] Arithmetic surface roughness (Ra) is defined in Equation 1. Z is the distance measured from an arbitrary zero plane and N is the number of measuring points.

$$\mathrm{Ra} = \frac{1}{N}\sum_{j=1}^{N}|Z_j| \tag{1}$$

AFM images and selected profiles of the substrate in dry state after polymerization are presented in **Figure 4**. Here as well, in each AFM image three topographical profiles (appear as white lines on the images with red, green and blue markers) are examined. The thickness along these profiles is presented below each image. The layer on the hot side (left) is, as expected, denser and thicker than on the cold side (right) with Ra values of 1.31 nm and 0.87 nm, accordingly. Absolute thickness values can be inferred from the selected profiles. While the thickness varies by up to 15 nm on the brush most populated side (left), it varies at most by few nanometers on the least populated side (right). Since the initial silanization is made over a broad range of temperatures, it is expected that the initiator molecules will tend to aggregate in some areas. These aggregates prior to polymerization are most likely to be enhanced afterward and appear as the higher spots in Figure 4. These areas, however, do not change significantly the overall properties (thickness, wettability) and they do not exceed 20 nm on the sparse side of the substrate, while on the dense part the aggregate height is 40 nm after polymerization.

4. Simulations of Heat Profiles in Silicon Wafers

The remarkable agreement between the resulting wetting properties of the BTPAm coated substrate and the temperature profile of the heated silicon wafer encouraged us to simulate other temperature gradients. The profiles can be tuned by changing the spacing between the heating stages and by changing the thickness of the silicon wafer as seen in **Figure 5**.

In order to compare between different profiles we introduce a parameter grad T, defined in Equation 2:

$$\mathrm{grad}T = \frac{\Delta T}{\Delta X}, \tag{2}$$

This parameter represents a derivative of temperature over the distance, and defines the slope or steepness of the gradient. We further consider the ideal case (no losses on heating stages) and model the thermal profiles for different spacing between the heating stages (l) and different heights in a silicon wafer of thickness d in the cases of thin ($d < l$) and thick ($d > l$) silicon wafer using the previously introduced parameter grad T.

In the former case, grad T = 11.6 kK m^{-1}, 8.8 kK m^{-1}, and 7 kK m^{-1} for distances of 2 mm, 4 mm, and 6 mm, respectively. It can be seen from these data that increasing the spacing l from 2 mm to 6 mm decreases the steepness of the gradient by almost 40%. Thus, with this relatively simple method one can attain powerful predictive capabilities, and this approach can be applied not only for the synthesis of gradient coatings, but also for the design of defined wetting properties of a substrate.

In the latter case, the thicker wafer ($d > l$) provides an indication of the temperature distribution for wafers of different thicknesses. The spacing between the heating stages l was kept constant. Here, thermal profiles and analysis of gradients were

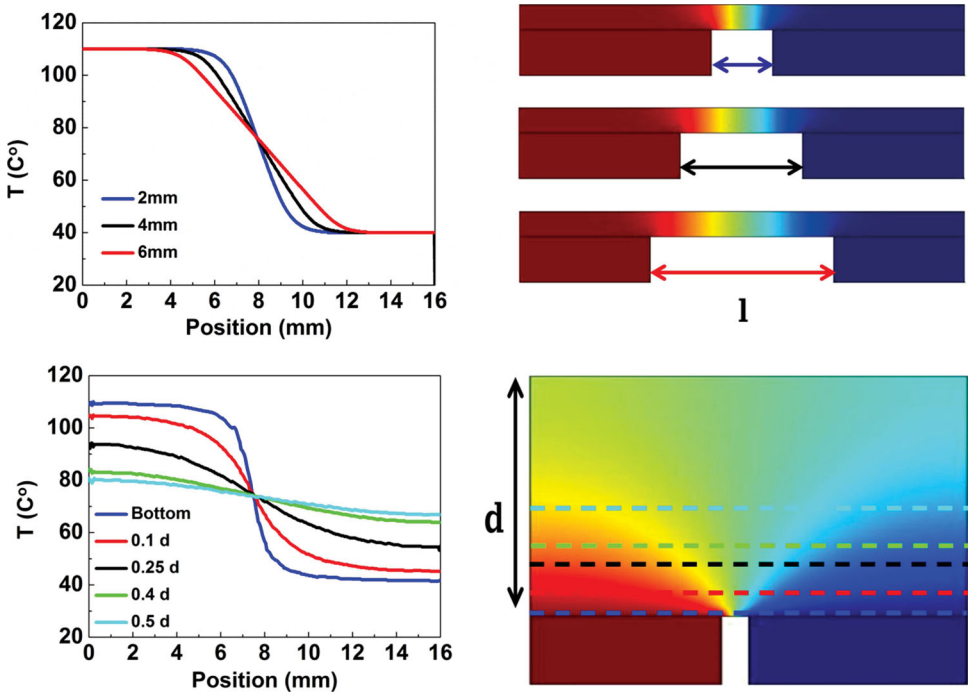

Figure 5. Top: simulated temperature profiles along a silicon wafer for various spacing between the heating stages- $l = 2$ mm, 4 mm and 6 mm (left) and heat distributions inside the wafers depending on the spacing (right). Bottom: temperature profiles inside a silicon wafer of thickness d, simulated for various distances from the heating stages- 0.1 d, 0.25 d, 0.4 d and 0.5 d (left) and the simulated heat distribution inside the silicon wafer (right). Dashed lines indicate distances from the heating stages corresponding to the heating profiles shown at the left-hand side.

extracted along the lines corresponding to 0.1 d, 0.25 d, 0.4 d, and 0.5 d (Figure 5, bottom). The values of grad T = 11.6 kK m^{-1}, 3.8 kK m^{-1}, 2.4 kK m^{-1}, 1.3 kK m^{-1}, and 0.8 kK m^{-1} were obtained from curves (left-hand side of Figure 6, bottom) for distances of 0.1 d, 0.25 d, 0.4 d, and 0.5 d, respectively, from the bottom surface as marked by dashed lines in the right-hand side panel of Figure 5, bottom. Thus, over one order of magnitude variation of the steepness of the gradient can be obtained with increasing the thickness of the silicon wafer.

It can be noted that changing the heating time changes the gradient profile as well, resulting in different contact angles as discussed in the supporting information (Figure S1, Supporting Information).

5. Conclusion

We have presented an easy and controllable method to assemble gradients of silane molecules and subsequently gradients of PAAm brushes polymerized from the silane template. A combinatorial approach has been used in our studies to map the influence of temperature on silanes spin-coated on substrates by applying thermal gradients. Heating is found to be a practical, facile and fast method for modification of silicon substrates without strict control of ambiance or water content in the silane solution. The wetting properties of the silicon substrate after the deposition of silane in this study are comparable with deposition from solution or vapor, however, are obtained within a time of 20 min. Furthermore, applying a thermal gradient is a useful tool for mapping and predicting the wetting properties, thickness, surface roughness and morphology of the PAAm brushes. The brush layer properties are largely influenced by the grafting density, determined by the silane initiator template. Hence, the final brush polymer thickness, roughness and wettability can be already determined by the initial deposition of the silane molecules. Because of good correlation between the applied temperature profile and the resulting silanization, simulations of the heat distribution inside the silicon wafers were performed to quantitatively extract additional profiles. We have introduced a simple method, based on the derivative of the temperature profile, which characterizes the steepness of the gradient distribution. These data were used for simulating temperature profiles of thin and thick (compared to the spacing between the heating pads) silicon slabs: based on agreement between experimental values and simulations, the desired surface wettability and polymer brush coverage can be predicted and tuned by these parameters. Thus, our studies can be applied to designing different wettability profiles, polymer and polymer brush coverage, which is of interest for designing different gradients, combinatorial analysis and elaborate surface coverage.[60,61]

6. Experimental Section

Materials: Highly polished single-crystal Si wafers of {100} orientation and 525 μm thickness were used as substrates. The wafers were first cleaned with Piranha solution (1:3 v/v, 30% H_2O_2:H_2SO_4. Handle with caution!). BTPAm (2-bromo-2-methyl-N-3-(triethoxysilyl) propyl

propanamide) was synthesized from (3-aminopropyl) triethoxysilane, 2-Bromo-2-methyl-propionyl bromide in DCM (Dichloromethane) according to a former protocol.[62] PAAm brushes were synthesized from AAm (Acrylamide), using Cu(|)Br, Byp (2,2'-Bipyridine) in water, based on a method from a former protocol.[63]

Gradient Synthesis: Clean silicon wafers of 17 mm × 10 mm were spin-coated (40 s, 4000 rpm) with BTPAm in toluene solution (1 m ^{M}). The Toluene was not anhydrous. The samples were put onto a custom made heating stage made of two computer-monitored Peltier plates with tunable temperature difference (Scheme 1). All steps were carried out at room temperature and ambiance. The ambient humidity was controlled and all experiments were performed at humidity values ranging between 36%–38%. with no humidity control. Finally, the samples were rinsed with vigorous flow of acetone and ethanol alternately, followed by sonication in toluene for 5 min at RT, 10% power. Wetting properties of the samples did not change over periods of days up to several weeks (more than that was not investigated). Nevertheless, for all samples polymerization took place immediately after initiator gradient preparation.

ATRP Polymerization: PAAm brushes were polymerized based on a previous report.[63] In brief, ATRP was initiated with an aqueous mixture of acrylamide/Cu(|)Br/byp (200:1:2 molar ratio). This reaction solution was boiled to decrease the air content prior to polymerization (see ATRP Polymerization Section in Supporting Information).[64] The polymerization was carried out at 80 °C for 24 h. The samples were washed 10 times with deionized water (DIW) after polymerization and dried under nitrogen.

Instruments: For BTPAm deposition, a spin-coater of Headway Research Inc., Texas, U.S.A, was used, while rinsing the samples was done in an ultrasonic bath of Bandelin (Sonorex super 10P digital). The water contact angle was measured with a Krüss G10 apparatus. For the temperature measurements, a custom made temperature sensor was used. Atomic Force microscope (AFM) images were recorded by a Veeco Multimode Nanoscope in tapping mode. Ellipsometry measurements were performed with a Multiskop from Optrel, Sinzing, Germany with a HeNe, 632.8 nm laser.

Simulation of Temperature Profiles: Simulation of temperature distribution was done using the COMSOL multiphysics software package. In the ideal case (no losses on heating stages) the temperature on the two heating stages was adjusted according to the set values. For example, for data shown by the blue continuous line in Figure 1 (and Figure 5) the higher temperature was set to 110 °C, while the lower temperature was set to 40 °C. To account for experimental data (the dashed blue line in Figure 1) we have fitted the data by splitting each of the heating stages into 3 sub-stages; the temperature fit produced 105, 103, and 101 °C at the higher temperature side, and 52, 43, and 40 °C at the lower temperature. The value for the thermal conductivity of silicon was 140 W m^{-1} K^{-1}.

Supporting Information

Supporting Information is available from the Wiley Online Library or from the author.

Acknowledgements

The authors thank Anne Heilig for the AFM imaging and Ursula Lubahn for technical support in the polymerizations. The authors also thank Dr. Stefan Karpitschka for valuable suggestions during the initial experiments and Dr. Filipe Vilela for assistance in the initiator synthesis. A.G.S. acknowledges the support of FWO of Belgium and BOF of University of Ghent.

Received: October 9, 2013
Revised: November 7, 2013
Published online: March 7, 2014

[1] I. Luzinov, S. Minko, V. V. Tsukruk, *Soft Matter* **2008**, *4*, 714–725.
[2] M. K. Chaudhury, G. M. Whitesides, *Science* **1992**, *256*, 1539–1541.
[3] G. Kumar, C.-C. Ho, C. C. Co, *Adv. Mater.* **2007**, *19*(8), 1084.
[4] M. S. Kim, G. Khang, H. B. Lee, *Prog. Polym. Sci.* **2008**, *33*(1), 138–164.
[5] C. G. Simon Jr., N. Eidelman, S. B. Kennedy, A. Sehgal, C. A. Khatri, *Biomaterials* **2005**, *26*(34), 6906.
[6] I. B. Burgess, N. Koay, K. P. Raymond, M. Kolle, M. Loncar, J. Aizenberg *ACS Nano* **2012**, *6*(2), 1427.
[7] R. R. Bhat, M. R. Tomlinson, J. Genzer, *J. Polym. Sci., Part B: Polym. Phys.* **2005**, *43*, 3384–3394.
[8] H. Elwing, S. Welin, A. Askendal, U. Nilsson, I. Lundstroem, *J. Colloid Interface Sci.* **1987**, *119*, 203–210.
[9] Y.-H. Chou, W.-Y. Lee, W.-C. Chen, *Adv. Funct. Mater.* **2012**, *22*, 4352–4359.
[10] Y.-H. Yu, C.-C. M. Ma, C.-C. Teng, Y.-L. Huang, S.-H. Lee, I. Wang, M.-H. Wei, *Mater. Chem. Phys.* **2012**, *136*(2–3), 334–340.
[11] C. E. Soteropulos, H. K. Hunt, *J. Vis. Exp.* **2012**, (63), e3866.
[12] L. Ionov, S. Minko, *ACS Appl. Mater. Interfaces* **2012**, *4*(1), 483–489.
[13] E. V. Skorb, H. Möhwald, *Adv. Mater.* **2013**, *25*(36),5029–43.
[14] S. Krackl, C. I. Someya, S. Enthaler, *Chem. – Eur. J.* **2012**, *18*(48), 15267–15271.
[15] M.-A. Tehfe, L. Ma, B. Graff, F. Morlet-Savary, J.-P. Fouassier, J. Zhao, J. Lalevée, *Macromol. Chem. Phys.* **2012**, *213*(21), 2282–2286.
[16] R. Jin, K. Liu, D. Xia, Q. Qian, G. Liu, H. Li, *Adv. Synth. Catal.* **2012**, *354*(17), 3265–3274.
[17] E. Nuhiji, C. S. Wong, A. Sutti, T. Lin, M. Kirkland, X. Wang, *ACS Appl. Mater. Interfaces* **2012**, *4*(6), 2912–2919.
[18] T. Wu, P. Gong, I. Szleifer, P. Vlcek, V. Subr, J. Genzer, *Macromolecules* **2007**, *40*(24), 8756–8764.
[19] N. C. Estillore, R. C. Advincula, *Macromol. Chem. Phys.* **2011**, *212*(15), 1552–1566.
[20] S. Peng, B. Bhushan, *R. Soc. Chem. Adv.* **2012**, *2*(23), 8557–8578.
[21] A. Ulman, *Chem. Rev.* **1996**, *96*(4), 1533–1554.
[22] I. Luzinov, D. Julthongpiput, A. Liebmann-Vinson, T. Cregger, M. D. Foster, V. V. Tsukruk, *Langmuir* **2000**, *16*(2), 504–516.
[23] M. Zhu, M. Z. Lerum, W. Chen, *Langmuir* **2012**, *28*(1), 416–423.
[24] D. W. Britt, V. Hlady, *J. Colloid Interface Sci.* **1996**, *178*(2), 775–784.
[25] Y. Liu, L. K. Wolf, M. C. Messmer, *Langmuir* **2001**, *17*(14), 4329–4335.
[26] A. N. Parikh, D. L. Allara, I. B. Azouz, F. Rondelez, *J. Phys. Chem.* **1994**, *98*, 7577–90.
[27] M. Zhu, M. Z. Lerum, W. Chen, *Langmuir* **2012**, *28*, 416–423.
[28] M. Zhu, M. Z. Lerum, W. Chen, *Langmuir* **2011**, *28*(1), 416–423.
[29] C. Cherkouk, L. Rebohle, W. Skorupa, T. Strache, H. Reuther, M. Helm, *J. Colloid Interface Sci.* **2009**, *337*(2), 375–380.
[30] Q. He, A. Kueller, S. Schilp, F. Leisten, H.-A. Kolb, M. Grunze, J. Li, *Small* **2007**, *3*(11), 1860–1865.
[31] Q. He, A. Kueller, M. Grunze, J. Li, *Langmuir* **2007**, *23*(7), 3981–3987.
[32] Q. He, Y. Tian, A. Kuller, M. Grunze, A. Golzhauser, J. Li, *J. Nanosci. Nanotechnol.* **2006**, *6*, 1838–1841.
[33] T. Solomun, R. Mix, H. Sturm, *ACS Appl. Mater. Interfaces* **2010**, *2*(8), 2171–2174.
[34] W. J. van Ooij, A. Sabata, *Surf. Interface Anal.* **1993**, *20*(5), 475–484.
[35] Y. Ito, A. A. Virkar, S. Mannsfeld, J. H. Oh, M. Toney, J. Locklin, Z. Bao, *J. Am. Chem. Soc.* **2009**, *131*(26), 9396–9404.
[36] W. Lin, S. Yitzchaik, W. Lin, A. Malik, M. K. Durbin, A. G. Richter, G. K. Wong, P. Dutta, T. J. Marks, *Angew. Chem. Int. Ed. Engl.* **1995**, *34*(13–14), 1497–1499.
[37] K. Hänni-Ciunel, G. H. Findenegg, R. Von Klitzing, *Soft Mater.* **2007**, *5*(2–3), 61–73.
[38] D. S. Salloum, S. G. Olenych, T. C. S. Keller, J. B. Schlenoff, *Biomacromolecules* **2005**, *6*(1), 161–167.

[39] S. V. Pavlukhina, J. B. Kaplan, L. Xu, W. Chang, X. Yu, S. Madhyastha, N. Yakandawala, A. Mentbayeva, B. Khan, S. A. Sukhishvili, *ACS Appl. Mater. Interfaces* **2012**, *4*(9), 4708–4716.
[40] X. He, W. Yang, X. Pei, *Macromolecules* **2008**, *13*(41), 4615–4621.
[41] M. J. Mulvihill, B. L. Rupert, R. He, A. Hochbaum, J. Arnold, P. Yang, *J. Am. Chem. Soc.* **2005**, *127*(46), 16040–16041.
[42] J. Li, H. Han, Q. Wang, X. Liu, S. Jiang, *J. Sep. Sci.* **2010**, *33*(17–18), 2804–2810.
[43] Y. Sun, X. Ding, Z. Zheng, X. Cheng, X. Hu, Y. Peng, *Eur. Polym. J.* **2007**, *43*(3), 762–772.
[44] M. Rutnakornpituk, N. Puangsin, P. Theamdee, B. Rutnakornpituk, U. Wichai, *Polymer* **2011**, *52*(4), 987–995.
[45] A. Ulman, *Chem. Rev.* **1996**, *96*, 1533–1554.
[46] R. Banga, J. Yarwood, A. M. Morgan, B. Evans, J. Kells, *Langmuir* **1995**, *11*, 4393–9.
[47] T. Wu, K. Efimenko, J. Genzer, *J. Am. Chem. Soc.* **2002**, *124*(32), 9394–9395.
[48] T. Wu, K. Efimenko, P. Vlcek, V. Subr, J. Genzer, *Macromolecules* **2003**, *36*, 2448–2453.
[49] J. Genzer, T. Wu, K. Efimenko, *Mater. Res. Soc. Symp. Proc., Mater. Res. Society* **2002**, *707* (Self-Assembly Processes in Materials), 9–14.
[50] Y. Zou, N. A. A. Rossi, J. N. Kizhakkedathu, D. E. Brooks, *Macromolecules* **2009**, *42*(13), 4817–4828.
[51] R. Iwata, R. Satoh, Y. Iwasaki, K. Akiyoshi, *Colloids Surf., B* **2008**, *62*(2), 288–298.
[52] J. Trmcic-Cvitas, E. Hasan, M. Ramstedt, X. Li, M. A. Cooper, C. Abell, W. T. S. Huck, J. E. Gautrot, *Biomacromolecules* **2009**, *10*(10), 2885–2894.
[53] S. Minko, S. Patil, V. Datsyuk, F. Simon, K.-J. Eichhorn, M. Motornov, D. Usov, I. Tokarev, M. Stamm, *Langmuir* **2002**, *18*(1), 289–296.
[54] I. Luzinov, D. Julthongpiput, H. Malz, J. Pionteck, V. V. Tsukruk, *Macromolecules* **2000**, *33*(3), 1043–1048.
[55] K. Rechendorff, M. B. Hovgaard, M. Foss, V. P. Zhdanov, F. Besenbacher, *Langmuir* **2006**, *22*(26), 10885–10888.
[56] V. P. Zhdanov, K. Rechendorff, M. B. Hovgaard, F. Besenbacher, *J. Phys. Chem. B* **2008**, *112*(24), 7267–7272.
[57] S. Munevar, Y.-L. Wang, M. Dembo, *Mol. Biol. Cell* **2001**, *12*, 3947–3954.
[58] K. Saha, J. Kim, E. Irwin, J. Yoon, F. Momin, V. Trujillo, D. V. Schaffer, K. E. Healy, R. C. Hayward, *Biophys. J.* **2010**, *99*(12), L94–L96.
[59] G. R. a. R. Ploeg, *Biomaterials in Modern Medicine, The Groningen Perspective* **2008**.
[60] R. B. Pernites, R. R. Ponnapati, R. C. Advincula, *Adv. Mater.* **2011**, *23*(28), 3207–3213.
[61] F. Boulmedais, C. S. Tang, B. Keller, J. Voros, *Adv. Funct. Mater.* **2006**, *16*(1), 63–70.
[62] M. J. Mulvihill, B. L. Rupert, R. He, A. Hochbaum, J. Arnold, P. Yang, *J. Am. Chem. Soc.* **2005**, *127*, 16040–16041.
[63] I. Fundeanu, H. C. van der Mei, A. J. Schouten, H. J. Busscher, *Colloids Surf., B* **2008**, *64*, 297–301.
[64] R. F. Weiss, *Deep-Sea Res. Oceanogr. Abstr.* **1970**, *17*(4), 721–735.